Intracerebral Nanoparticle Transport Facilitated by Alzheimer Pathology and Age

Gregory C. Tracy[1,*], **Kai-Yu Huang**[2,*], **Yu-Tong Hong**[2,*], **Shengzhe Ding**[2], **Hayden A. Noblet**[1,5], **Ki H. Lim**[1], **Eung Chang Kim**[1], **Hee Jung Chung**[1,3,4,5,#], **Hyunjoon Kong**[2,3,4,5,6,#]

[1]Department of Molecular and Integrative Physiology, University of Illinois at Urbana-Champaign, Urbana, IL 61801, USA

[2]Department of Chemical and Biomolecular Engineering, University of Illinois at Urbana-Champaign, Urbana, IL 61801, USA

[3]Beckman Institute for Advanced Science and Technology, University of Illinois at Urbana-Champaign, Urbana, IL 61801, USA

[4]Carl R. Woese Institute for Genomic Biology, University of Illinois at Urbana-Champaign, Urbana, IL 61801, USA

[5]Neuroscience Program, University of Illinois at Urbana-Champaign, Urbana, IL 61801, USA.

[6]KU-KIST Graduate School of Converging Science and Technology, Korea University, Seongbuk-gu, Seoul 02841, South Korea

Abstract

Nanoparticles have emerged as potential transporters of drugs targeting Alzheimer's disease (AD), but their design should consider the blood-brain barrier (BBB) integrity and neuroinflammation of the AD brain. This study presents that aging is a significant factor for the brain localization and retention of nanoparticles which we engineered to bind with reactive astrocytes and activated microglia. We assembled 200 nm-diameter particles using a block copolymer of poly(lactic-co-glycolic acid) (PLGA) and CD44-binding hyaluronic acid (HA). The resulting PLGA-b-HA nanoparticles displayed increased binding to CD44-expressing reactive astrocytes and activated microglia. Upon intravascular injection, nanoparticles were localized to the hippocampi of both

ASSOCIATED CONTENT
Supporting Information
The Supporting Information is available free of charge at https://pubs.acs.org/.
Details of materials and methods, characterization of synthesized PLGA-b-HA, and toxicity tests of PLGA-b-HA nanoparticle

APP/PS1 AD model mice and their control littermates at 13–16 months of age due to enhanced transvascular transport through leaky BBB. No particles were found in the hippocampi of young adult mice. These findings demonstrate the brain localization of nanoparticles due to aging-induced BBB breakdown, regardless of the AD pathology.

Graphical Abstract
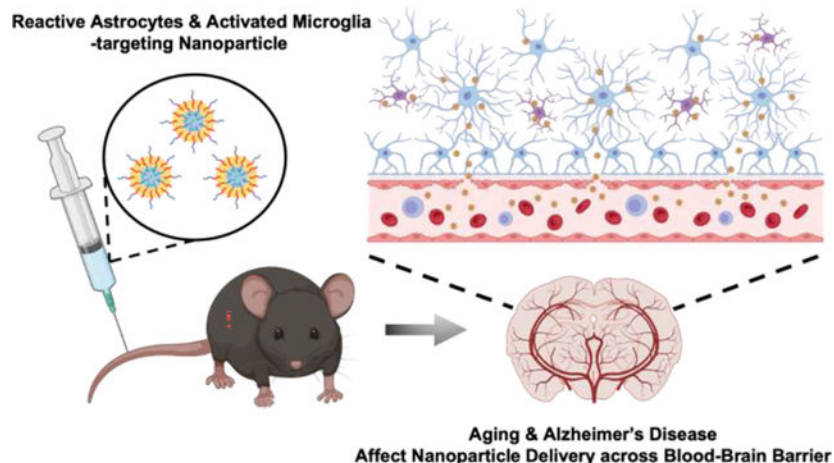
Keywords

PLGA nanoparticles; Alzheimer's disease; reactive astrocytes; hyaluronic acid; aging

A variety of neurodegenerative diseases affect more than 270 million people globally, claiming the second leading cause of death[1]. Among neurodegenerative diseases that cause mild cognitive impairment (MCI) and dementia, Alzheimer's disease (AD) is the most common cause of dementia in older adults. AD is characterized by progressive and irreversible memory loss with neuronal atrophy starting typically from the hippocampus[2]. AD prevalence and its associated mortality are expected to rise with increases in population and age[3]. In AD, accumulation of extracellular senile amyloid-β (Aβ) plaques and intracellular neurofibrillary tangles composed of hyperphosphorylated tau are associated with synapse loss and neurodegeneration. Extensive efforts have been made to mitigate the loss of synapses and neurons, and ultimately alleviate cognitive decline. These efforts include stem cell transplantation[4, 5], immunotherapy, and small molecule drugs that can decrease these molecular hallmarks of AD, such as inhibiting the Aβ aggregation[6–9]. However, most small molecule drugs show promising results in *in vitro* cell culture and preclinical animal studies, but often fail in clinical studies[10, 11], partly because of off-target effects, the loss of their activity in the brain, or limited transport to the brain due to poor solubility in body fluids[12, 13].

To improve the bioavailability and retention of therapeutic drug molecules in the brain, biofunctionalized nanoparticles have emerged as promising hydrophobic drug transporters for treating various diseases[14], as they confer flexibilities in modulating their geometry and properties[15–17]. Several strategies have been developed to enhance the efficacy of

nanocarriers in transporting drugs across the BBB. These include engineering the size and charge of the nanoparticles, as well as conjugating ligands[18, 19]. Nanoparticles smaller than a 200 nm diameter have been shown to cross over capillaries which become more permeable with injuries and diseases due to the enhanced permeability and retention effect.

There is increasing evidence that many neurodegenerative diseases, including AD, are associated with BBB disruption. The normal BBB maintains brain homeostasis by mediating the restricted solute exchange between the blood circulation and the brain parenchyma and prevents unwanted toxins and pathogens from entering the brain. This barrier, however, breaks down with age and in many neurodegenerative diseases, resulting in increased BBB permeability and immune cell infiltration[20–23]. For instance, magnetic resonance images (MRI) show microhemorrhages in the brains of AD patients[24]. The BBB-impermeable MRI contrast agent, gadolinium, can enter the brains of patients with MCI[25], indicative of leaky BBB. Anatomical studies of endothelial cells in the postmortem brain tissues of AD patients show reductions in tight junction proteins and pericytes[21, 23, 26, 27], indicative of compromised BBB integrity. Since aging is a major risk factor for neurodegenerative diseases including AD, the disrupted BBB in aged brains and neurodegenerative diseases offers a chance to deliver therapeutic drug molecules by intravascular administration.

However, whether AD pathology coupled with aging enhances transvascular transport of nanoparticles via the disrupted BBB has yet to be examined systematically. Furthermore, small nanoparticles can be drained out quickly by the glymphatic flow right after movement from blood to the brain [28–30]. Hence, nanoparticle transport and retention are significantly affected by the brain pathology and microenvironment [30, 31]. However, to date, how compromised vascular integrity and the extravascular microenvironment of the aged and diseased brain affect the localization and retention of nanoparticles remains unanswered.

In this study, we hypothesized that aging, AD pathology, or both would increase the BBB permeability and neuroinflammation, thereby enhancing the transport of nanoparticles. In addition, nanoparticles engineered to bind to reactive astrocytes and activated microglia would remain in the brain following the transvascular transport (Fig. 1A). To test this hypothesis, we assembled 200 nm-diameter nanoparticles with a block copolymer of poly(lactic-co-glycolic acid) (PLGA) and hyaluronic acid (HA)[32]. The HA units on the resulting PLGA-b-HA nanoparticles can bind to CD44 proteins[33] which are highly expressed on the surface membrane of reactive astrocytes and activated microglia compared to neurons[34, 35]. We delivered the nanoparticles via intravascular injections to young adult and aged (13–16 months) wild-type mice and APP/PS1 AD model mice which overproduces Aβ[36] and displays the BBB disruption starting at 4 months of age and the severe BBB leakage by 9 months of age[37, 38]. We then examined systemic biodistribution and toxicity of nanoparticles and their localization in the hippocampus, the key brain region that shows significant neurodegeneration and neuroinflammation in AD[20, 39, 40]. We uncover that the brain localization and retention of nanoparticles are attributed to the aging-induced BBB breakdown and neuroinflammation, respectively, regardless of the presence of extracellular Aβ plaques.

We synthesized PLGA-b-HA by conjugating the carboxylate group of PLGA and the primary amine group of aminated HA (Fig. S1A). The resulting PLGA-b-HA dispersed in D_2O showed HA-characteristic peaks at 1.8 ppm (N-acetyl group) and 2.9–4.5 ppm (methylene and glucosidic protons) in the ^1H NMR spectra (Fig. S1B). In contrast, the same polymer dispersed in DMSO exhibited PLGA-characteristic peaks at 1.47, 4.91, and 5.21 ppm, representing the methyl, methylene, and (–OCH(CH$_3$)CO–) group, respectively (Fig. S1B). These results confirm the linkage between PLGA and HA blocks throughout the synthesis.

The PLGA-b-HA nanoparticles encapsulating fluorescent Alexa Fluor (AF) 488-conjugated BSA were prepared via double emulsification (Fig. 1B). The resulting nanoparticles are in the form of spheres with an average diameter of 206 ± 49 nm according to the transmission electron microscope (TEM) image (Fig. 1C) and dynamic light scattering (Fig. 1D). In particular, the TEM image confirms a bi-layered structure on the PLGA-b-HA particles, in which hydrophobic PLGA fills cores while the hydrophilic HA layer surrounds the PLGA core.

Chronic brain inflammation is a key feature of AD, with reactive astrocytes and activated microglia being evident in the early stage of AD[20, 40]. To examine if PLGA-b-HA nanoparticles can preferentially bind to reactive astrocytes, mouse cortical neural stem cells (NSCs) were differentiated into a monolayer culture of astrocytes (Fig. 2A). NSC-derived astrocytes were activated with 50 ng/mL tumor necrosis factor-α (TNF-α). Compared to control treatment, TNF-α stimulated the CD44 expression in astrocytes and led to thicker astrocytic branches (Fig. 2A). Specifically, TNF-α increased the CD44 mRNA level by 6-fold and CD44 protein expression by 2.3-fold (Fig 2B–C), consistent with the previous report[41]. Next, TNF-α-treated and untreated astrocytes were incubated with PLGA or PLGA-b-HA nanoparticles containing AF488-conjugated BSA (Fig 2D). Confocal fluorescence imaging revealed that the number of PLGA-b-HA nanoparticles bound on TNF-α-treated astrocytes was 4.5 times greater than those bound to untreated astrocytes (Fig 2E) and 4 times higher than PLGA particles (Fig 2F).

Microglial activation also stands out in Alzheimer's disease (AD) [20], and CD44 is expressed in activated microglia[35]. Upon activation, these microglia release inflammatory mediators, such as TNF-α, interleukin 1-beta, and interleukin-6, potentially leading to neuron damage[42]. To assess whether PLGA-b-HA nanoparticles could bind to activated microglia, mouse microglia were treated for 24 h with 10 ng/mL lipopolysaccharide (LPS), a well-known model for triggering neuroinflammation[43]. LPS upregulated CD44 expression in microglia (Fig 2G–H) and increased cellular secretion of TNF-α (Fig 2I). In addition, LPS-activated microglia exhibited a 1.9-fold higher binding affinity for the PLGA-b-HA nanoparticles encapsulating AF488-conjugated BSA than untreated cells (Fig 2J–K).

To test the neurotoxicity of PLGA-b-HA particles, we incubated primary rat hippocampal neuronal culture at DIV 10 with various concentrations of PLGA-b-HA particles (Fig. S2). After 3 h incubation, the metabolic activity of neurons was examined by a colorimetric MTT assay. According to the International Organization for Standardization (ISO 10993–5), the nanoparticle treatment is considered non-toxic when >70% metabolic activity is observed

compared to untreated cells. We found that PLGA-b-HA particles at concentrations of 0.04, 0.08, 0.16, and 0.62 mg/mL retained > 70% metabolic activity of cultured neurons (Fig. S2). With these results, PLGA-b-HA particles at < 0.62 mg/mL are expected to be safe for the following *in vivo* study.

To test if PLGA-b-HA particles can cross the BBB and localize to the brain, adult C57BL/6J mice at 3–5 months of age were intravenously (i.v.) injected via tail vein with saline (negative control) or PLGA-b-HA particles (16 mg/kg) filled with AF647-conjugated BSA. The chosen dose is 3.88-fold lower than the dose at which metabolic activity decreases below 70% (Fig. S2). At 2 h post-injection, various organs were rapidly dissected, and the particle distribution in these dissected organs was immediately examined by IVIS imaging. In the particle-injected young adult C57BL/6J mice, we observed strong AF647 fluorescence signal only in their liver but not in other organs, including the brain (Fig. 3A–B). No fluorescence signal was detected in the dissected organs of the saline-injected mice (Fig. 3A–B).

To monitor transvascular transport and localization of PLGA-b-HA nanoparticles due to increased BBB permeability and CD44-expression in reactive astrocytes and activated microglia[20, 26, 39], we chose a transgenic APP/PS1 mouse model (APPSwe/PSEN1dE9). This model expresses both a chimeric mouse/human amyloid precursor protein (APP) gene harboring a Swedish mutation (K670N/M671L) and a mutant human presenilin-1 (PSEN1) carrying the deletion of exon 9 (dE9) driven by the mouse prion promoter[44]. This model displays high levels of soluble Aβ oligomers, neuroinflammation (microgliosis, reactive astrocytes) starting at 3 months of age [45], synapse loss starting at 5 months of age, visible Aβ plaque deposition, synaptic plasticity defects, and memory loss at 6–7 months of age[36, 46, 47], and significant BBB disruption and permeability by 9 months of age [38].

We repeated i.v. injections of PLGA-b-HA particles (16 mg/kg) containing AF647-conjugated BSA into the APP/PS1 mice and their non-carrier (NC) control littermates at 3–5 months of age, which is considered "young adults", as well as at 15–17 months of age, which is considered "old aged" [48]. IVIS imaging at 2 h post-injection detected significant fluorescence in the brains of both APP/PS1 mice and their NC littermates at 15–17 months of age compared to APP/PS1 mice and their NC littermates at 3–5 months of age or saline-injected C57BL/6J mice at 3–5 months of age (Fig. 3A–B), indicating the enhanced brain localization of PLGA-b-HA particles in the aged APP/PS1 and NC mice. However, aged APP/PS1 mice showed significantly more particles in their brains compared to the aged NC mice as well as young adult APP/PS1 mice (Fig. 3A–B). Interestingly, increased fluorescence intensities were also evident in the heart, lung, and liver of aged APP/PS1 mice compared to saline-injected young adult C57BL/6J mice (Fig. 3A–B), demonstrating enhanced localization of PLGA-b-HA particles in these organs upon aging and AD pathology (Fig. 3A–B).

The hippocampus is critical for learning and memory that is affected early in AD and is the major site for neurodegeneration and neuroinflammation in AD[39, 49]. Following i.v. injections of saline or PLGA-b-HA nanoparticles containing AF488-conjugated BSA, the 30 μm thick cryosections of their formaldehyde-fixed brains were subjected to immunostaining

for Aβ and confocal imaging for Aβ plaques and nanoparticles. Aged APP/PS1 mice showed abundant Aβ plaques in the CA1, CA3, and DG regions of their hippocampi whereas Aβ plaques were minimal in aged-match NC control mice, young adult APP/PS1 and NC mice, and young adult C57BL/6J mice (Fig. 4A).

Consistent with IVIS imaging (Fig. 3), particle-injected aged APP/PS1 mice displayed significant numbers of fluorescent puncta in their hippocampal CA1 ($p<0.001$ and $p<0.001$), CA3 ($p<0.05$ and $p<0.01$), and DG ($p<0.01$ and $p<0.001$) regions compared to saline- and particle-injected young adult C57BL/6J mice, respectively, both of which showed minimal fluorescent puncta (Fig. 4B–C). Compared to saline- and particle-injected C57BL/6J mice, NC controls at 13–16 months of age also displayed significant numbers of fluorescent puncta in all hippocampal regions, which were similar to those in their aged-match APP/PS1 mice (Fig. 4B–C), demonstrating that PLGA-b-HA nanoparticles localized to the hippocampi of 13–16-month-old mice regardless of Aβ overexpression.

We also assessed the potential toxicity of the PLGA-b-HA nanoparticles. Two hours post-i.v. injections with either saline or the nanoparticles (16 mg/kg) containing AF488- or AF647-conjugated BSA, whole blood samples and serum samples were collected for white blood cell analysis (Table S1) and chemistry profiling (Fig S3), respectively. The total number of white blood cells in mice administered with either saline or the nanoparticles remained comparable and within the normal range (Table S1)[50]. The composition of white blood cells was consistent across both groups. In serum, the levels of creatinine and blood urea nitrogen (BUN) remained similar between saline- and particle-injected groups (Fig S3A–B), indicating stable kidney function. The serum levels of alkaline phosphatase (ALP), alanine aminotransferase (ALT), albumin, and globulin were also comparable in both groups, indicating normal liver function (Fig S3C–F). These analyses confirmed that PLGA-b-HA nanoparticles do not stimulate immune cells in the blood and minimally impact kidney and liver functions.

Localization of PLGA-b-HA particles to the hippocampi of aged mice regardless of AD pathology suggest that BBB disruption and permeability might have occurred even in NC control mice at 13–16 months of age. To test this possibility, aged APP/PS1 mice and their NC littermates received intravascular injections of fluorescein isothiocyanate (FITC)-labeled dextran, which is widely used to determine the BBB permeability by examining their leakage to the surrounding parenchyma. Confocal imaging detected weak but significant fluorescence signal in the hippocampi of FITC-dextran-injected young adult C57BL/6J mice compared to saline-injected control mice (Fig. 5A–B). Furthermore, we observed significantly stronger FITC-dextran signals in the hippocampi of both aged APP/PS1 mice and their non-carrier littermates compared to FITC-dextran-injected young adult C57BL/6J mice (Fig. 5A), with a small genotype difference seen only in the hippocampal CA1 region (Fig. 5B). These data support the presence of the BBB leakage in the hippocampi of aged mice regardless of the genotype.

Nanoparticles have been previously reported to target inflammation in osteoarthritis[51] and lung cancer[52]. However, whether nanoparticles can localize across the BBB into the brain parenchyma and target inflammation-inflicted brain regions was unclear. This study

shows that PLGA-b-HA particles with an average diameter of 206 ± 49 nm can bind to reactive astrocytes and microglia with minimal neurotoxicity in primary culture. We further provide evidence that intravascularly injected PLGA-b-HA particles localize to the hippocampi of both aged APP/PS1 AD model mice and their control littermates due to increased BBB leakage. However, the particle localization to the hippocampi of young adult C57BL6/J mice was minimal. Importantly, these particles did not induce notable immune responses or cause acute adverse effects on liver and kidney. Such AD pathology and aging-dependent brain targeting of PLGA-b-HA nanoparticles due to increased BBB breakdown and neuroinflammation supports their broad application as drug carriers for aging-associated neurodegenerative diseases.

Our IVIS and confocal imaging analyses in young adult C57BL/6J mice at 2–5 months of age revealed very low BBB permeation of FITC-dextran and no PLGA-b-HA particle signals in their hippocampi at 2 h post intravascular injection (Figs. 3–5). Similarly, minimal PLGA-b-HA particle signals were detected in the hippocampi of young adult APP/PS1 mice at 4–5 months of age (Fig. 4). Consistent with our findings, unmodified PLGA nanoparticles have been shown to cross the BBB primarily through passive internalization based on size[53] but have a 5% BBB permeation rate *in vitro* and low BBB penetration *in vivo* in wild-type rats[54]. In addition to low BBB permeability, high rate of their clearance through the reticuloendothelial system[53] and rapid removal of HA by endothelial cells of the liver sinusoids[55] could underlie the minimal localization of PLGA-b-HA particles in the young adult mouse brain (Figs. 3 & 4). Interestingly, intravascularly-injected PLGA-b-HA particles were found mostly in the livers of young adult mice with minimal localization to their hearts, spleens, and kidneys (Fig. 3), suggesting the particle retention specifically in the liver despite the large amounts of free particles in the systemic circuitry.

In contrast to the young adult C57BL/6J, NC, and APP/PS1 mice, significant amounts of FITC-dextran and PLGA-b-HA nanoparticles were found in the hippocampi of NC control mice at 18 and 13–16 months of age, respectively, at 2 h post i.v. injection (Figs. 4 & 5). As artificially disrupting the BBB by using a hyperosmotic solution or cytotoxic agents has also shown to increase nanoparticle penetration across the BBB[56, 57], these results suggest that aging increases the BBB permeability and the brain penetration of nanoparticles. Indeed, compromised BBB integrity has been reported in 12-month-old C57BL/6J mice[58] and healthy but older humans at 47–91 years of age[59]. Age-dependent BBB breakdown begins in the hippocampus[60], and is associated with cognitive decline and neuroinflammation[61]. Thus, increased neuroinflammation in aged mice could also help retain PLGA-b-HA nanoparticles in the brain since CD44 is the primary cell surface receptor for HA[62] and is highly expressed in reactive microglia and activated astrocytes during neuroinflammation[35]. HA also binds to the receptor for hyaluronan-mediated cell motility (RHAMM) that is expressed in the astrocytes in the subventricular zone (SVZ)[63]. Therefore, the localization of PLGA-b-HA nanoparticles in the hippocampus of aged APP/PS1 mice and their control littermates could also be facilitated by their initial binding to RHAMM-positive astrocytes followed by astrocyte migration from the SVZ to the hippocampus.

Pathological molecular hallmarks of AD are extracellular senile Aβ plaques, intracellular neurofibrillary tangles, and chronic neuroinflammation characterized by reactive astrocytes

and microglia infiltration[2, 40]. AD patients also display increased BBB permeability[26, 37, 61]. Increased neuroinflammation in the hippocampus of the AD brain is expected to facilitate the transvascular transport and binding of PLGA-b-HA particles to CD44-expressing reactive astrocytes and activated microglia, thereby increasing their retention at the inflammation-rich hippocampus. Indeed, our IVIS imaging showed a greater PLGA-b-HA particle localization in the brains of APP/PS1 mice than NC control mice at 15–17 months of age upon intravascular injection (Fig. 3), consistent with previous studies that demonstrated an increase in BBB permeability in the brains of two AD mouse models (5xFAD and APP/PS1) compared to their control littermates at 9 months of age[38, 64], which is considered pre-middle age[48].

However, we observed that the extent of BBB permeability and PLGA-b-HA localization in the hippocampi of APP/PS1 mice was similar to those in their NC control littermates at 13–16 months of age (Figs. 4 & 5), although the extracellular Aβ senile plaques were only seen in the hippocampi of APP/PS1 mice but not those of the control mice (Fig. 4A). As the hippocampus is affected early in AD and is the major site for neurodegeneration and neuroinflammation in AD[39, 49], we speculate that the level of BBB permeability and neuroinflammation in the hippocampi compared to the entire brain might have been advanced in our control NC mice due to the aging to a similar extent as APP/PS1 mice at 13–17 months of age which corresponds to the range between middle age and old age. Nonetheless, increased BBB permeability in old C57BL/6J mice[65](Fig. 5) would facilitate the transport of nanoparticles across the BBB for the delivery of drugs against aging-associated neurologic disorders and neurodegenerative diseases.

We also propose that HA blocks of PLGA-b-HA nanoparticles facilitate the transvascular transport of nanoparticles. Conjugated HA units prevent aggregation of PLGA nanoparticles in blood, thus supporting the transport of particles into the brain through the permeable BBB in the APP/PS1 mouse and their control littermates at 13–17 months. We did not test unmodified PLGA nanoparticles because the i.v. injection often caused death, likely due to uncontrolled aggregation of nanoparticles in blood.

In addition, the PLGA-b-HA nanoparticles can be further modified to enable active targeting of the BBB in the AD brain. For example, HA blocks can be conjugated with peptides binding to the transferrin receptor[66] or lactoferrin receptor[67]. Such binding has been shown to activate receptor-mediated transcytosis of nanoparticles[67]. PLGA-b-HA nanoparticles can also be functionalized with brain-targeting peptides, identified from the unbiased screening of phage libraries to improve organ selectivity[68]. Moreover, nanoparticles can be conjugated with galactose to target glucose transporter 1 to facilitate the particle penetration of BBB via glycemia-controlled glucose transporter-1 recycling and deliver small interfering RNAs (siRNAs) against β-site APP cleavage enzyme 1 (BACE1) that can reverse cognitive deficit in APP/PS1 mice[69]. Lastly, coating the particles with lectin[70] or hexadecyltrimethylammonium bromide[71] can increase a positive surface charge and prolong the duration of the particle retention on luminal surfaces of the BBB against high shear stress on the vascular wall[53]. Future studies shall explore these active BBB-targeting strategies that can facilitate particle delivery into the brain.

Supplementary Material

Refer to Web version on PubMed Central for supplementary material.

FUNDING

DATA AVAILABILITY STATEMENT

The datasets generated and analyzed for this study will be uploaded as to the appropriate data repository and the link will be provided upon the acceptance of this study.

REFERENCES

1. Collaborators GBDN, Global, regional, and national burden of neurological disorders, 1990–2016: a systematic analysis for the Global Burden of Disease Study 2016. Lancet Neurol 2019, 18 (5), 459–480. [PubMed: 30879893]

2. McKhann G; Drachman D; Folstein M; Katzman R; Price D; Stadlan EM, Clinical diagnosis of Alzheimer's disease: report of the NINCDS-ADRDA Work Group under the auspices of Department of Health and Human Services Task Force on Alzheimer's Disease. Neurology 1984, 34 (7), 939–44. [PubMed: 6610841]

3. 2021 Alzheimer's disease facts and figures. Alzheimers Dement 2021, 17 (3), 327–406. [PubMed: 33756057]

4. Espuny-Camacho I; Arranz AM; Fiers M; Snellinx A; Ando K; Munck S; Bonnefont J; Lambot L; Corthout N; Omodho L; Vanden Eynden E; Radaelli E; Tesseur I; Wray S; Ebneth A; Hardy J; Leroy K; Brion J-P; Vanderhaeghen P; De Strooper B, Hallmarks of Alzheimer's Disease in Stem-Cell-Derived Human Neurons Transplanted into Mouse Brain. Neuron 2017, 93 (5), 1066–1081.e8. [PubMed: 28238547]

5. Yu D; Zhang H; Liu Z; Liu C; Du X; Ren J; Qu X, Hydrogen-Bonded Organic Framework (HOF)-Based Single-Neural Stem Cell Encapsulation and Transplantation to Remodel Impaired Neural Networks. Angewandte Chemie International Edition 2022, 61 (28), e202201485. [PubMed: 35385196]

6. Karran E; Mercken M; De Strooper B, The amyloid cascade hypothesis for Alzheimer's disease: an appraisal for the development of therapeutics. Nat Rev Drug Discov 2011, 10 (9), 698–712. [PubMed: 21852788]

7. Bloom GS, Amyloid-beta and tau: the trigger and bullet in Alzheimer disease pathogenesis. JAMA Neurol 2014, 71 (4), 505–8. [PubMed: 24493463]

8. Khanna MR; Kovalevich J; Lee VM; Trojanowski JQ; Brunden KR, Therapeutic strategies for the treatment of tauopathies: Hopes and challenges. Alzheimers Dement 2016, 12 (10), 1051–1065. [PubMed: 27751442]

9. Du Z; Li M; Ren J; Qu X, Current Strategies for Modulating Aβ Aggregation with Multifunctional Agents. Accounts of Chemical Research 2021, 54 (9), 2172–2184. [PubMed: 33881820]

10. Cummings JL; Morstorf T; Zhong K, Alzheimer's disease drug-development pipeline: few candidates, frequent failures. Alzheimers Res Ther 2014, 6 (4), 37. [PubMed: 25024750]

11. Golde TE; Schneider LS; Koo EH, Anti-abeta therapeutics in Alzheimer's disease: the need for a paradigm shift. Neuron 2011, 69 (2), 203–13. [PubMed: 21262461]

12. Smith DE; Johanson CE; Keep RF, Peptide and peptide analog transport systems at the blood-CSF barrier. Adv Drug Deliv Rev 2004, 56 (12), 1765–91. [PubMed: 15381333]

13. Eyal S; Hsiao P; Unadkat JD, Drug interactions at the blood-brain barrier: fact or fantasy? Pharmacol Ther 2009, 123 (1), 80–104. [PubMed: 19393264]

14. Wang AZ; Gu F; Zhang L; Chan JM; Radovic-Moreno A; Shaikh MR; Farokhzad OC, Biofunctionalized targeted nanoparticles for therapeutic applications. Expert Opin Biol Ther 2008, 8 (8), 1063–70. [PubMed: 18613759]

15. Patra JK; Das G; Fraceto LF; Campos EVR; Rodriguez-Torres MDP; Acosta-Torres LS; Diaz-Torres LA; Grillo R; Swamy MK; Sharma S; Habtemariam S; Shin HS, Nano based drug delivery systems: recent developments and future prospects. J Nanobiotechnology 2018, 16 (1), 71. [PubMed: 30231877]

16. Pelaz B; Alexiou C; Alvarez-Puebla RA; Alves F; Andrews AM; Ashraf S; Balogh LP; Ballerini L; Bestetti A; Brendel C; Bosi S; Carril M; Chan WC; Chen C; Chen X; Chen X; Cheng Z; Cui D; Du J; Dullin C; Escudero A; Feliu N; Gao M; George M; Gogotsi Y; Grunweller A; Gu Z; Halas NJ; Hampp N; Hartmann RK; Hersam MC; Hunziker P; Jian J; Jiang X; Jungebluth P; Kadhiresan P; Kataoka K; Khademhosseini A; Kopecek J; Kotov NA; Krug HF; Lee DS; Lehr CM; Leong KW; Liang XJ; Ling Lim M; Liz-Marzan LM; Ma X; Macchiarini P; Meng H; Mohwald H; Mulvaney P; Nel AE; Nie S; Nordlander P; Okano T; Oliveira J; Park TH; Penner RM; Prato M; Puntes V; Rotello VM; Samarakoon A; Schaak RE; Shen Y; Sjoqvist S; Skirtach AG; Soliman MG; Stevens MM; Sung HW; Tang BZ; Tietze R; Udugama BN; VanEpps JS; Weil T; Weiss PS; Willner I; Wu Y; Yang L; Yue Z; Zhang Q; Zhang Q; Zhang XE; Zhao Y; Zhou X; Parak WJ, Diverse Applications of Nanomedicine. ACS Nano 2017, 11 (3), 2313–2381. [PubMed: 28290206]

17. Jain A; Jain SK, Ligand-Appended BBB-Targeted Nanocarriers (LABTNs). Crit Rev Ther Drug Carrier Syst 2015, 32 (2), 149–80. [PubMed: 25955883]

18. Hersh AM; Alomari S; Tyler BM, Crossing the Blood-Brain Barrier: Advances in Nanoparticle Technology for Drug Delivery in Neuro-Oncology. International Journal of Molecular Sciences 2022, 23 (8), 4153. [PubMed: 35456971]

19. Zhou Y; Peng Z; Seven ES; Leblanc RM, Crossing the blood-brain barrier with nanoparticles. Journal of Controlled Release 2018, 270, 290–303. [PubMed: 29269142]

20. Maccioni RB; Rojo LE; Fernandez JA; Kuljis RO, The role of neuroimmunomodulation in Alzheimer's disease. Ann N Y Acad Sci 2009, 1153, 240–6. [PubMed: 19236346]

21. Sweeney MD; Sagare AP; Zlokovic BV, Blood-brain barrier breakdown in Alzheimer disease and other neurodegenerative disorders. Nat Rev Neurol 2018, 14 (3), 133–150. [PubMed: 29377008]

22. Cortes-Canteli M; Zamolodchikov D; Ahn HJ; Strickland S; Norris EH, Fibrinogen and altered hemostasis in Alzheimer's disease. J Alzheimers Dis 2012, 32 (3), 599–608. [PubMed: 22869464]

23. Hendriksen E; van Bergeijk D; Oosting RS; Redegeld FA, Mast cells in neuroinflammation and brain disorders. Neurosci Biobehav Rev 2017, 79, 119–133. [PubMed: 28499503]

24. Devanarayan P; Devanarayan V; Llano DA; Alzheimer's Disease Neuroimaging I, Identification of a Simple and Novel Cut-Point Based Cerebrospinal Fluid and MRI Signature for Predicting Alzheimer's Disease Progression that Reinforces the 2018 NIA-AA Research Framework. J Alzheimers Dis 2019, 68 (2), 537–550. [PubMed: 30775985]

25. Llano DA; Devanarayan P; Devanarayan V; Alzheimer's Disease Neuroimaging I, VGF in Cerebrospinal Fluid Combined With Conventional Biomarkers Enhances Prediction of Conversion From MCI to AD. Alzheimer Dis Assoc Disord 2019, 33 (4), 307–314. [PubMed: 31305322]

26. Sweeney MD; Zhao Z; Montagne A; Nelson AR; Zlokovic BV, Blood-Brain Barrier: From Physiology to Disease and Back. Physiol Rev 2019, 99 (1), 21–78. [PubMed: 30280653]

27. Mahoney ER; Dumitrescu L; Moore AM; Cambronero FE; De Jager PL; Koran MEI; Petyuk VA; Robinson RAS; Goyal S; Schneider JA; Bennett DA; Jefferson AL; Hohman TJ, Brain expression of the vascular endothelial growth factor gene family in cognitive aging and alzheimer's disease. Mol Psychiatry 2021, 26 (3), 888–896. [PubMed: 31332262]

28. Louveau A; Plog BA; Antila S; Alitalo K; Nedergaard M; Kipnis J, Understanding the functions and relationships of the glymphatic system and meningeal lymphatics. J Clin Invest 2017, 127 (9), 3210–3219. [PubMed: 28862640]

29. Plog BA; Nedergaard M, The Glymphatic System in Central Nervous System Health and Disease: Past, Present, and Future. Annu Rev Pathol 2018, 13, 379–394. [PubMed: 29195051]

30. Kwak B; Ozcelikkale A; Shin CS; Park K; Han B, Simulation of complex transport of nanoparticles around a tumor using tumor-microenvironment-on-chip. J Control Release 2014, 194, 157–67. [PubMed: 25194778]

31. Sassaroli E; O'Neill BE, Modulation of the interstitial fluid pressure by high intensity focused ultrasound as a way to alter local fluid and solute movement: insights from a mathematical model. Phys Med Biol 2014, 59 (22), 6775–95. [PubMed: 25327766]

32. Teo JY; Seo Y; Ko E; Leong J; Hong YT; Yang YY; Kong H, Surface tethering of stem cells with H(2)O(2)-responsive anti-oxidizing colloidal particles for protection against oxidation-induced death. Biomaterials 2019, 201, 1–15. [PubMed: 30784768]

33. Dzwonek J; Wilczynski GM, CD44: molecular interactions, signaling and functions in the nervous system. Front Cell Neurosci 2015, 9, 175. [PubMed: 25999819]

34. Lagos-Cabre R; Alvarez A; Kong M; Burgos-Bravo F; Cardenas A; Rojas-Mancilla E; Perez-Nunez R; Herrera-Molina R; Rojas F; Schneider P; Herrera-Marschitz M; Quest AFG; van Zundert B; Leyton L, alpha(V)beta(3) Integrin regulates astrocyte reactivity. J Neuroinflammation 2017, 14 (1), 194. [PubMed: 28962574]

35. Sosunov AA; Guilfoyle E; Wu X; McKhann GM 2nd; Goldman JE, Phenotypic conversions of "protoplasmic" to "reactive" astrocytes in Alexander disease. J Neurosci 2013, 33 (17), 7439–50. [PubMed: 23616550]

36. Trinchese F; Liu S; Battaglia F; Walter S; Mathews PM; Arancio O, Progressive age-related development of Alzheimer-like pathology in APP/PS1 mice. Ann Neurol 2004, 55 (6), 801–14. [PubMed: 15174014]

37. Wang Q; Huang X; Su Y; Yin G; Wang S; Yu B; Li H; Qi J; Chen H; Zeng W; Zhang K; Verkhratsky A; Niu J; Yi C, Activation of Wnt/beta-catenin pathway mitigates blood-brain barrier dysfunction in Alzheimer's disease. Brain 2022, 145 (12), 4474–4488. [PubMed: 35788280]

38. Kelly P; McClean PL; Ackermann M; Konerding MA; Holscher C; Mitchell CA, Restoration of cerebral and systemic microvascular architecture in APP/PS1 transgenic mice following treatment with Liraglutide. Microcirculation 2015, 22 (2), 133–45. [PubMed: 25556713]

39. Guzman-Martinez L; Maccioni RB; Andrade V; Navarrete LP; Pastor MG; Ramos-Escobar N, Neuroinflammation as a Common Feature of Neurodegenerative Disorders. Front Pharmacol 2019, 10, 1008. [PubMed: 31572186]

40. Chun H; Lee CJ, Reactive astrocytes in Alzheimer's disease: A double-edged sword. Neurosci Res 2018, 126, 44–52. [PubMed: 29225140]

41. Gabel S; Koncina E; Dorban G; Heurtaux T; Birck C; Glaab E; Michelucci A; Heuschling P; Grandbarbe L, Inflammation Promotes a Conversion of Astrocytes into Neural Progenitor Cells via NF-kappaB Activation. Mol Neurobiol 2016, 53 (8), 5041–55. [PubMed: 26381429]

42. Hansen DV; Hanson JE; Sheng M, Microglia in Alzheimer's disease. Journal of Cell Biology 2017, 217 (2), 459–472. [PubMed: 29196460]

43. Skrzypczak-Wiercioch A; Sałat K, Lipopolysaccharide-Induced Model of Neuroinflammation: Mechanisms of Action, Research Application and Future Directions for Its Use. Molecules 2022, 27 (17), 5481. [PubMed: 36080253]

44. Savonenko A; Xu GM; Melnikova T; Morton JL; Gonzales V; Wong MP; Price DL; Tang F; Markowska AL; Borchelt DR, Episodic-like memory deficits in the APPswe/PS1dE9 mouse model of Alzheimer's disease: relationships to beta-amyloid deposition and neurotransmitter abnormalities. Neurobiol Dis 2005, 18 (3), 602–17. [PubMed: 15755686]

45. van Tijn P; Dennissen FJ; Gentier RJ; Hobo B; Hermes D; Steinbusch HW; Van Leeuwen FW; Fischer DF, Mutant ubiquitin decreases amyloid beta plaque formation in a transgenic mouse model of Alzheimer's disease. Neurochem Int 2012, 61 (5), 739–48. [PubMed: 22797007]

46. Megill A; Tran T; Eldred K; Lee NJ; Wong PC; Hoe HS; Kirkwood A; Lee HK, Defective Age-Dependent Metaplasticity in a Mouse Model of Alzheimer's Disease. J Neurosci 2015, 35 (32), 11346–57. [PubMed: 26269641]

47. Jacobsen JS; Wu CC; Redwine JM; Comery TA; Arias R; Bowlby M; Martone R; Morrison JH; Pangalos MN; Reinhart PH; Bloom FE, Early-onset behavioral and synaptic deficits in a mouse model of Alzheimer's disease. Proc Natl Acad Sci U S A 2006, 103 (13), 5161–6. [PubMed: 16549764]

48. Flurkey K; Currer JM; Harrison D, Mouse models in aging research. In The mouse in biomedical research, Elsevier: 2007; pp 637–672.

49. Nicoll RA, A Brief History of Long-Term Potentiation. Neuron 2017, 93 (2), 281–290. [PubMed: 28103477]

50. White JR; Gong H; Colaizy TT; Moreland JG; Flaherty H; McElroy SJ, Evaluation of hematologic variables in newborn C57/BL6 mice up to day 35. Veterinary Clinical Pathology 2016, 45 (1), 87–95. [PubMed: 26717267]

51. Zerrillo L; Gigliobianco MR; D'Atri D; Garcia JP; Baldazzi F; Ridwan Y; Fuentes G; Chan A; Creemers LB; Censi R; Di Martino P; Cruz LJ, PLGA Nanoparticles Grafted with Hyaluronic Acid to Improve Site-Specificity and Drug Dose Delivery in Osteoarthritis Nanotherapy. Nanomaterials (Basel) 2022, 12 (13).

52. Wu J; Deng C; Meng F; Zhang J; Sun H; Zhong Z, Hyaluronic acid coated PLGA nanoparticulate docetaxel effectively targets and suppresses orthotopic human lung cancer. J Control Release 2017, 259, 76–82. [PubMed: 28027947]

53. Zhi K; Raji B; Nookala AR; Khan MM; Nguyen XH; Sakshi S; Pourmotabbed T; Yallapu MM; Kochat H; Tadrous E; Pernell S; Kumar S, PLGA Nanoparticle-Based Formulations to Cross the Blood-Brain Barrier for Drug Delivery: From R&D to cGMP. Pharmaceutics 2021, 13 (4).

54. Chen YC; Hsieh WY; Lee WF; Zeng DT, Effects of surface modification of PLGA-PEG-PLGA nanoparticles on loperamide delivery efficiency across the blood-brain barrier. J Biomater Appl 2013, 27 (7), 909–22. [PubMed: 22207601]

55. Laurent TC; Fraser JR, Hyaluronan. FASEB J 1992, 6 (7), 2397–404. [PubMed: 1563592]

56. Nair M; Jayant RD; Kaushik A; Sagar V, Getting into the brain: Potential of nanotechnology in the management of NeuroAIDS. Adv Drug Deliv Rev 2016, 103, 202–217. [PubMed: 26944096]

57. Haluska M; Anthony ML, Osmotic blood-brain barrier modification for the treatment of malignant brain tumors. Clin J Oncol Nurs 2004, 8 (3), 263–7. [PubMed: 15208820]

58. Takechi R; Pallebage-Gamarallage MM; Lam V; Giles C; Mamo JC, Aging-related changes in blood-brain barrier integrity and the effect of dietary fat. Neurodegener Dis 2013, 12 (3), 125–35. [PubMed: 23128303]

59. Verheggen ICM; de Jong JJA; van Boxtel MPJ; Gronenschild E; Palm WM; Postma AA; Jansen JFA; Verhey FRJ; Backes WH, Increase in blood-brain barrier leakage in healthy, older adults. Geroscience 2020, 42 (4), 1183–1193. [PubMed: 32601792]

60. Montagne A; Barnes SR; Sweeney MD; Halliday MR; Sagare AP; Zhao Z; Toga AW; Jacobs RE; Liu CY; Amezcua L; Harrington MG; Chui HC; Law M; Zlokovic BV, Blood-brain barrier breakdown in the aging human hippocampus. Neuron 2015, 85 (2), 296–302. [PubMed: 25611508]

61. Bowman GL; Dayon L; Kirkland R; Wojcik J; Peyratout G; Severin IC; Henry H; Oikonomidi A; Migliavacca E; Bacher M; Popp J, Blood-brain barrier breakdown, neuroinflammation, and cognitive decline in older adults. Alzheimers Dement 2018, 14 (12), 1640–1650. [PubMed: 30120040]

62. Lesley J; Hascall VC; Tammi M; Hyman R, Hyaluronan binding by cell surface CD44. J Biol Chem 2000, 275 (35), 26967–75. [PubMed: 10871609]

63. Pibuel MA; Poodts D; Molinari Y; Díaz M; Amoia S; Byrne A; Hajos S; Lompardía S; Franco P, The importance of RHAMM in the normal brain and gliomas: physiological and pathological roles. British journal of cancer 2023, 128 (1), 12–20. [PubMed: 36207608]

64. Ahn KC; Learman CR; Dunbar GL; Maiti P; Jang WC; Cha HC; Song MS, Characterization of Impaired Cerebrovascular Structure in APP/PS1 Mouse Brains. Neuroscience 2018, 385, 246–254. [PubMed: 29777753]

65. Elahy M; Jackaman C; Mamo JC; Lam V; Dhaliwal SS; Giles C; Nelson D; Takechi R, Blood-brain barrier dysfunction developed during normal aging is associated with inflammation and loss of tight junctions but not with leukocyte recruitment. Immun Ageing 2015, 12, 2. [PubMed: 25784952]

66. Huang N; Lu S; Liu XG; Zhu J; Wang YJ; Liu RT, PLGA nanoparticles modified with a BBB-penetrating peptide co-delivering Abeta generation inhibitor and curcumin attenuate memory

deficits and neuropathology in Alzheimer's disease mice. Oncotarget 2017, 8 (46), 81001–81013. [PubMed: 29113362]

67. Yu Y; Pang Z; Lu W; Yin Q; Gao H; Jiang X, Self-assembled polymersomes conjugated with lactoferrin as novel drug carrier for brain delivery. Pharm Res 2012, 29 (1), 83–96. [PubMed: 21979908]

68. Li J; Feng L; Fan L; Zha Y; Guo L; Zhang Q; Chen J; Pang Z; Wang Y; Jiang X; Yang VC; Wen L, Targeting the brain with PEG-PLGA nanoparticles modified with phage-displayed peptides. Biomaterials 2011, 32 (21), 4943–50. [PubMed: 21470674]

69. Zhou Y; Zhu F; Liu Y; Zheng M; Wang Y; Zhang D; Anraku Y; Zou Y; Li J; Wu H; Pang X; Tao W; Shimoni O; Bush AI; Xue X; Shi B, Blood-brain barrier–penetrating siRNA nanomedicine for Alzheimer's disease therapy. Science Advances 2020, 6 (41), eabc7031. [PubMed: 33036977]

70. Piazza J; Hoare T; Molinaro L; Terpstra K; Bhandari J; Selvaganapathy PR; Gupta B; Mishra RK, Haloperidol-loaded intranasally administered lectin functionalized poly(ethylene glycol)-block-poly(D,L)-lactic-co-glycolic acid (PEG-PLGA) nanoparticles for the treatment of schizophrenia. Eur J Pharm Biopharm 2014, 87 (1), 30–9. [PubMed: 24560967]

71. Platel A; Carpentier R; Becart E; Mordacq G; Betbeder D; Nesslany F, Influence of the surface charge of PLGA nanoparticles on their in vitro genotoxicity, cytotoxicity, ROS production and endocytosis. J Appl Toxicol 2016, 36 (3), 434–44. [PubMed: 26487569]
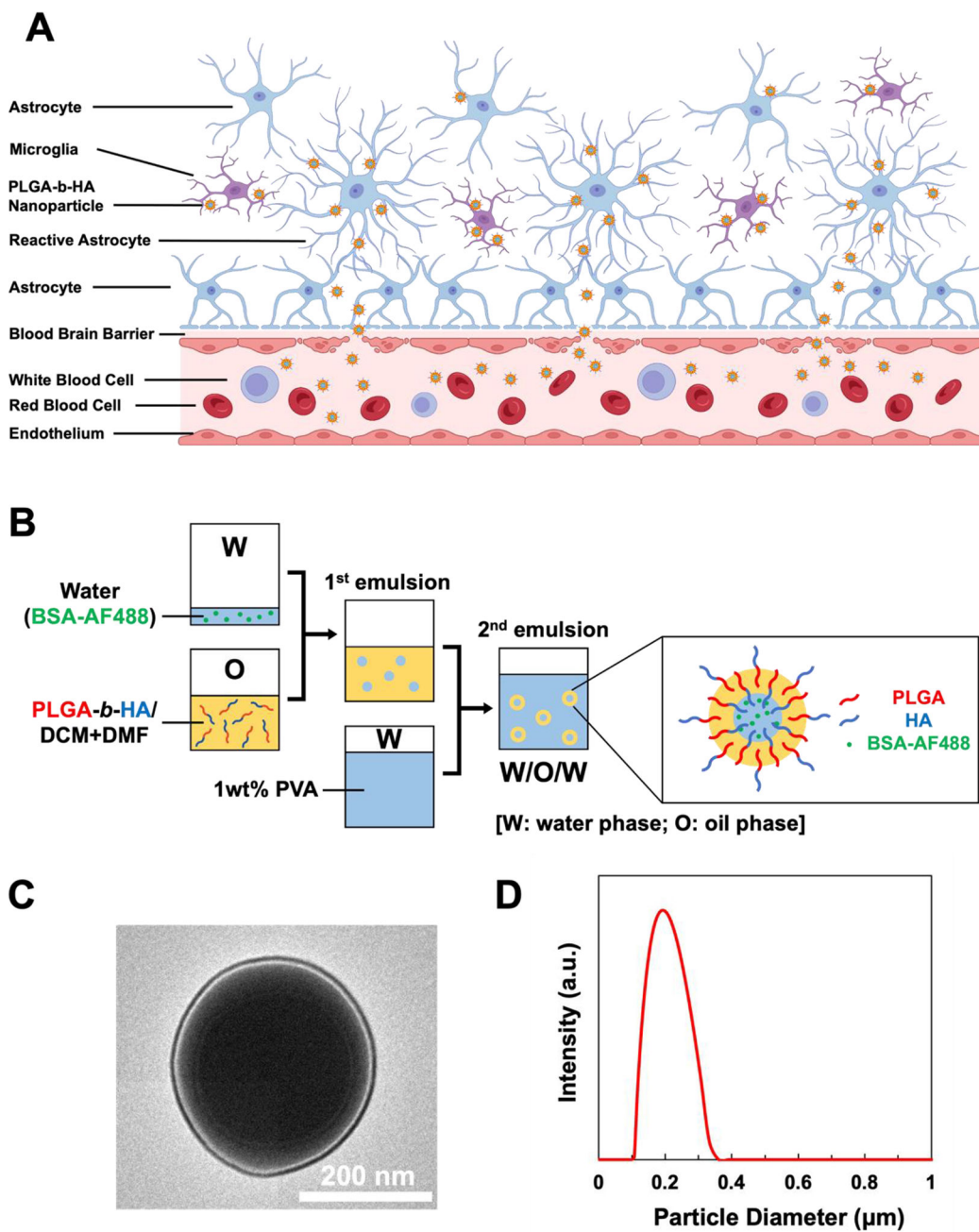
Figure 1. Synthesis and Characterization of PLGA-b-HA nanoparticles.
(**A**) A schematic illustration of PLGA-b-HA nanoparticles penetrating the blood-brain barrier (BBB) in aged or diseased conditioned and their subsequent binding to the reactive astrocytes and microglia. Created with BioRender.com (**B**) Illustration of double emulsion process to prepare PLGA-b-HA particles encapsulating AF488-conjugated BSA (W: water phase; O: oil phase). (**C**) Transmission electron microscopic image of PLGA-b-HA nanoparticle. (**D**) Size distribution of PLGA-b-HA nanoparticles analyzed via dynamic light scattering.
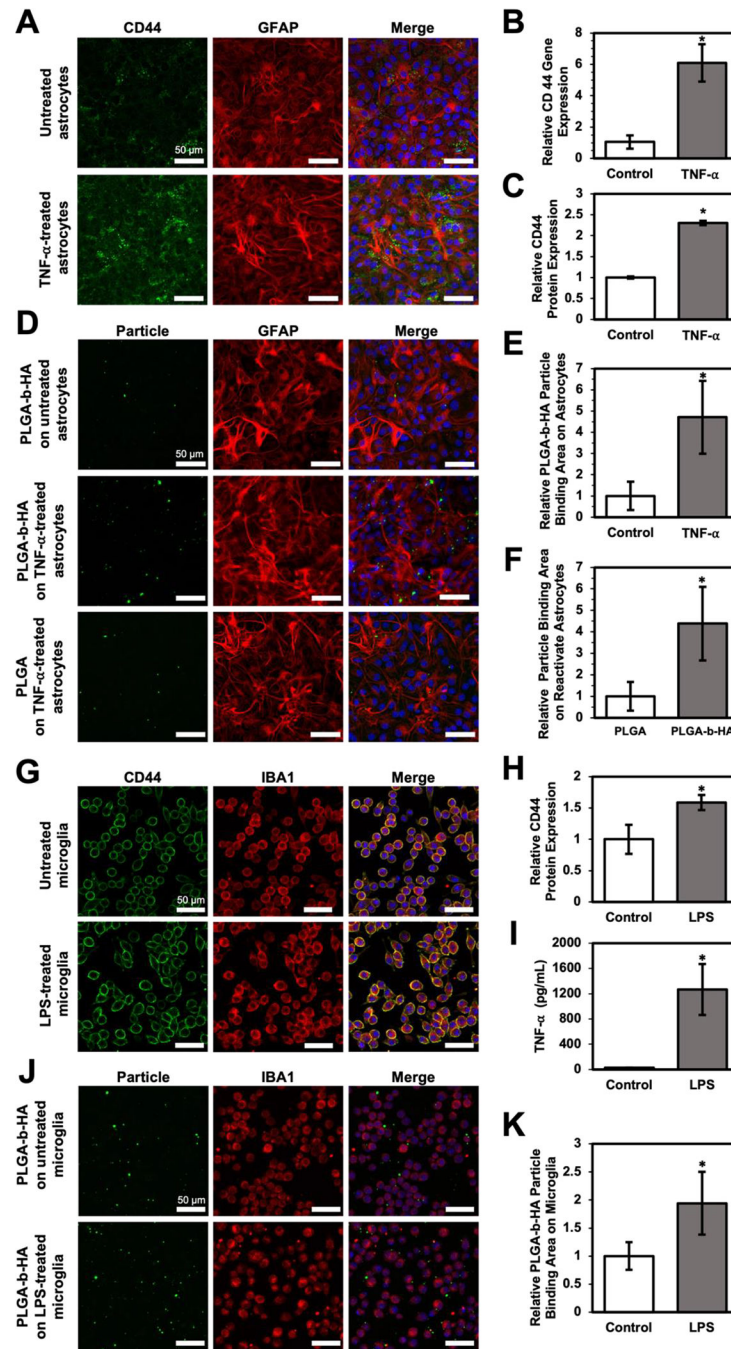
Figure 2. PLGA-b-HA particles preferentially bind to TNF-α-stimulated reactive astrocytes and LPS-stimulated microglia that express CD44.

(**A**) TNFα-activated CD44 expression of NSC-derived astrocytes. Immunofluorescence images of astrocytes without or with 24 h TNF-α treatment. Astrocytes were labeled with GFAP antibody (red), CD44 was labeled with CD44 antibody (green), and nuclei were stained with DAPI (blue). (**B**) Relative CD44-encoding mRNA expression level and (**C**) CD44 expression area of NSCs-derived astrocyte without (Control) and with TNF-α treatment. (**D**) Immunofluorescence images of nanoparticles associating with reactive or

untreated astrocytes. 0.5 mg/mL of PLGA particles or PLGA-b-HA particles were incubated with untreated or TNF-α-treated astrocytes for 20 minutes. Both PLGA and PLGA-b-HA particles were encapsulated with AF488 (Green)-conjugated BSA. Astrocytes were colored in red, and the nuclei were labeled in blue. **(E)** Quantitative analysis of PLGA-b-HA nanoparticles bound to astrocytes treated with/without TNF-α. The binding area of the PLGA-b-HA particles was normalized to the binding area observed on untreated astrocytes. **(F)** Quantitative analysis of PLGA and PLGA-b-HA nanoparticle bound to TNF-α-treated astrocytes. Particle binding area on activated astrocytes was normalized to that of PLGA particles. **(G)** LPS enhanced CD44 expression of microglia. Immunofluorescence images of microglia after 24 hours without or with 10 ng/mL LPS stimulation. Microglia were labeled with IBA1 antibody(red), CD44 was labeled with CD44 antibody (green), and nuclei were stained with DAPI (blue). **(H)** Relative CD44 expression area normalized by microglia cell number without (Control) and with hours LPS treatment (LPS). (n > 8, * = p < 0.05) **(I)** TNF-α concentration in the medium of microglia cultured without (Control) and with LPS for 24 hours (LPS). (n = 3, * = p < 0.05) **(J)** Immunofluorescence images of particles binging to LPS-treated microglia. PLGA-b-HA particles encapsulating AF 488-conjugated BSA were incubated with untreated or LPS-treated microglia for 20 minutes. Particles binding to the microglia were presented in green, microglia were presented in red, and the nucleus were presented in blue. **(K)** Analysis of PLGA-b-HA particle binding area on microglia without (Control) or with LPS treatment (LPS). The binding area was divided by total cell number in each view and normalized to the value of the control group. (n > 8, * = p < 0.05) Data represent the mean ± SEM. Unpaired Student t-test results are shown (n > 4, *p < 0.05).
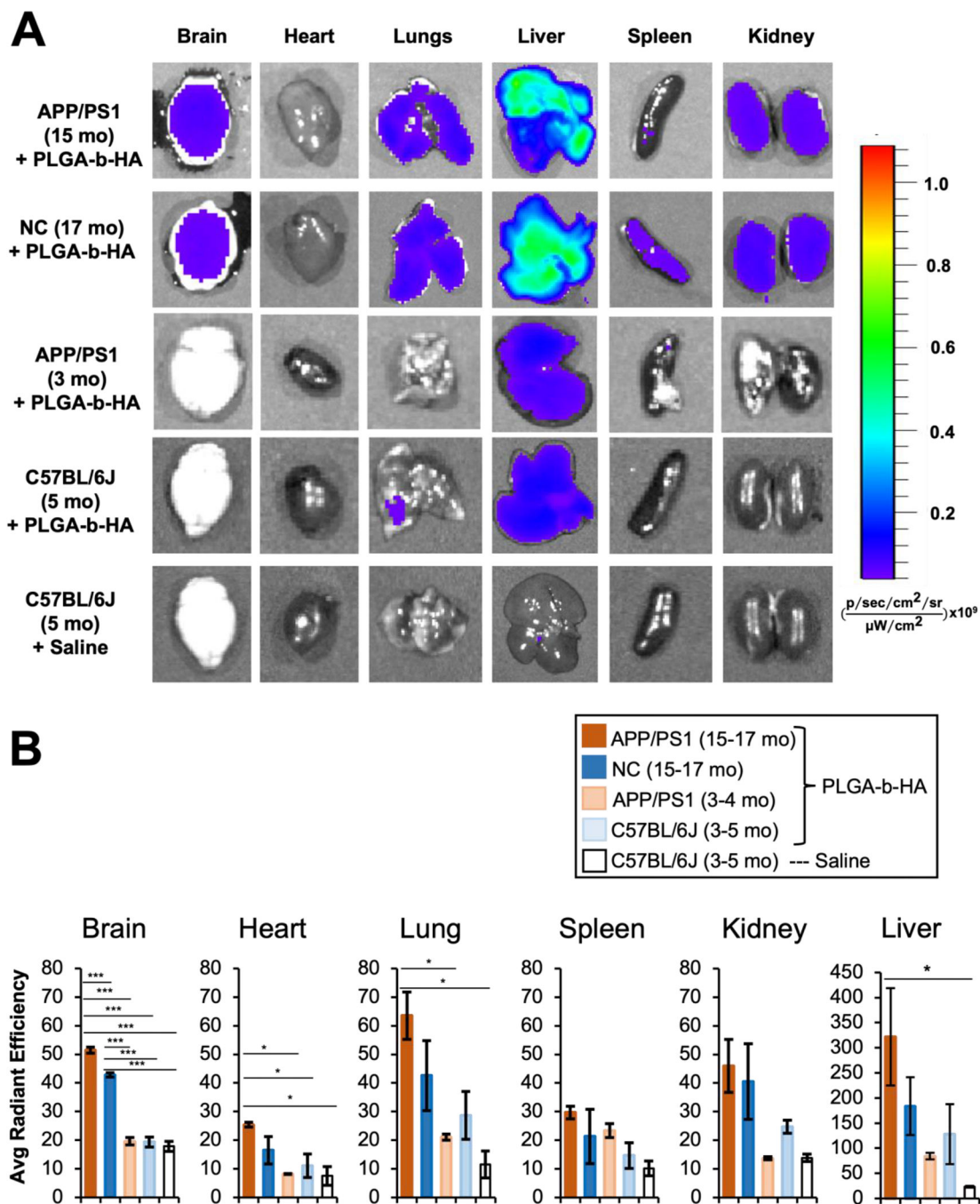
Figure 3. Intravenously injected PLGA-b-HA nanoparticles localize to the brain in aged APP/PS1 and control mice but not young adult mice.

Mice received an i.v. injection of saline or PLGA-b-HA particles encapsulating AF647-conjugated BSA (Dose: 16 mg/kg). At 2 h post injection, various organs were quickly dissected and imaged using IVIS. All images were taken with an excitation wavelength of 640 nm and an emission wavelength of 680 nm. **(A)** Representative *ex vivo* fluorescence images of the organs of 3–5-month-old wild-type mice receiving saline (n = 3 mice), 5-month-old young C57BL/6J mice receiving fluorescent PLGA-b-HA particles (n = 3

mice), 3–4-month-old young APP/PS1 mice receiving fluorescent PLGA-b-HA particles (n = 3 mice), 15–17-month-old APP/PS1 mice receiving fluorescent PLGA-b-HA particles (n = 3 mice), and 15–17-month-old non-carrier (NC) control littermates receiving fluorescent PLGA-b-HA particles (n = 3 mice). **(B)** Quantification of particle fluorescent intensity per unit area in brain and other organs. Data represents the mean ± SEM. One-way ANOVA with Tukey Post Hoc test results are shown (*p<0.05; ***p<0.001).
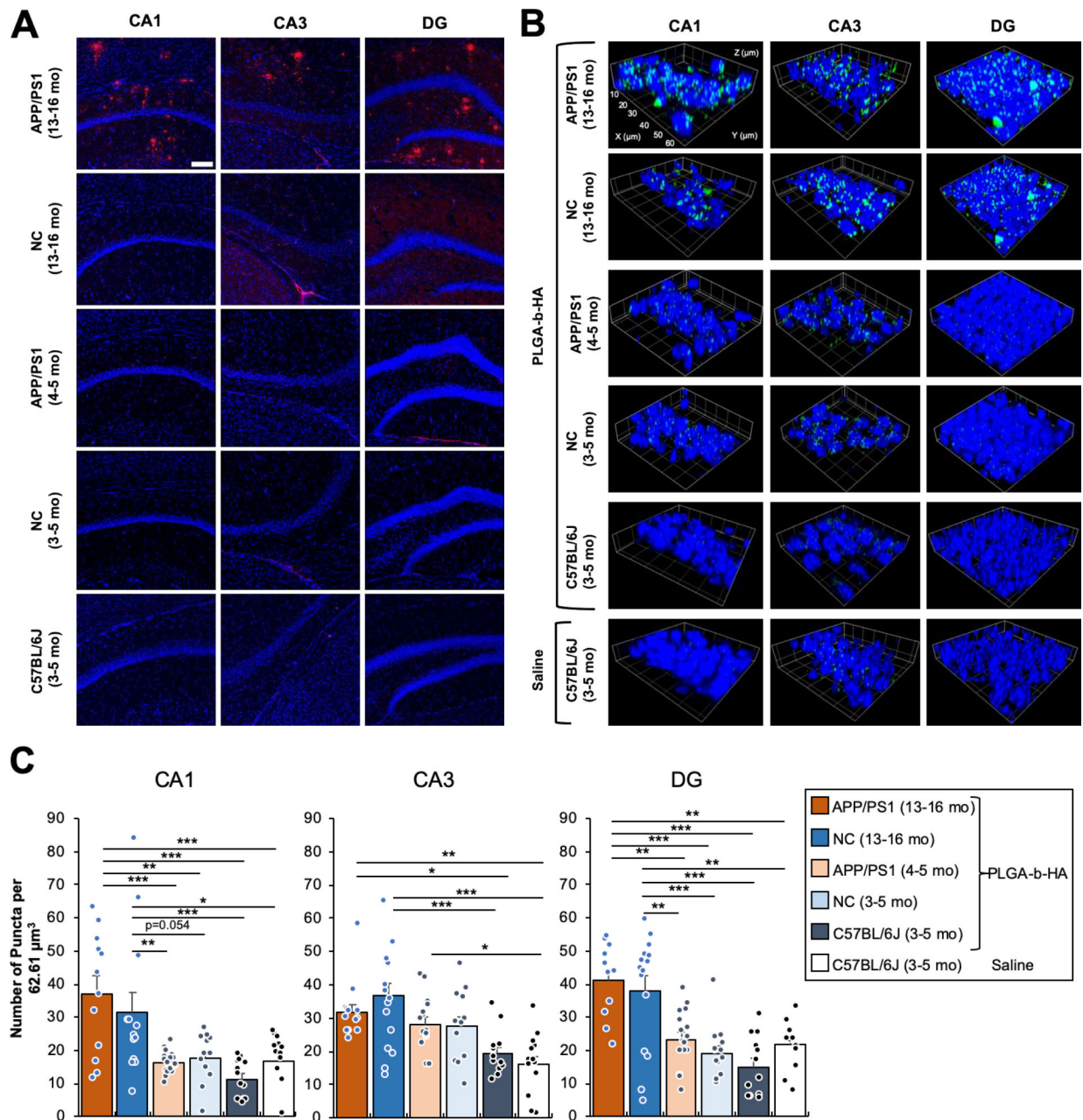
Figure 4. Intravenously injected PLGA-b-HA nanoparticles localize to the hippocampi of both aged APP/PS1 mice and their control littermates but not young adult mice.

(A) Coronal brain cryosections were immunostained for Aβ and counterstained with nuclear marker Hoechst 33342. Extracellular senile Aβ plaques were observed in all areas of the hippocampi of aged APP/PS1 mice (13–16-month-old), but not in the age-matched non-carrier (NC) mice (13–16-month-old) or young APP/PS1, NC control, and C57BL/6J mice (3–5-month-old). Confocal z-stack images (an optical section of 1.0 μm) were collected from the CA1, CA3, and Dente gyrus (DG) regions of the hippocampus and shown as representative images. Image size: 640.17 μm x 640.17 μm. Scale bar: 100μm. **(B)** Young adult APP/PS1, NC control littermates, and C57BL/6J mice (3–5 mo old), and aged

APP/PS1 mice and their NC control littermates (13–17 mo old) received an i.v. injection of saline or PLGA-b-HA particles encapsulating AF488-conjugated BSA (16 mg / kg) via their tail veins. After 2 h, mice were subjected to transcardial perfusion of PBS followed by fixation with 2% PFA. Cryoprotected brain tissues were sectioned to 30 μm coronal sections and counterstained with nuclear marker Hoechst 33342. Confocal images (an optical section of 1.0 μm) were collected from the CA1, CA3, and Dente gyrus (DG) regions of the hippocampus. Image size: 62.68 μm x 62.68 μm x 1.0 μm. Scale: each inset square is 10 μm x 10 μm. **(C)** Quantification of the average number of particles. Data represents the mean ± SEM. Particles are counted when artificial unit (AU) intensity is 5 standard deviations above the mean intensity for each image using the ThunderStorm plug-in with ImageJ. Sample size in CA1 (z-stack images and particle-injected mice): n = 12 from 3 aged APP/PS1 mice, n = 13 from 3 aged NC mice, n = 22 from 3 adult APP/PS1 mice, n = 12 from 3 adult NC mice, and n = 13 from 3 adult C57BL/6J mice. Sample size in CA3 (z-stack images and particle-injected mice): n = 13 from 3 aged APP/PS1 mice, n = 16 from 3 aged NC mice, n = 15 from 3 adult APP/PS1 mice, n = 12 from 2 adult NC mice, n = 12 from 3 adult C57BL/6J mice. Sample size in DG (z-stack images and particle-injected mice): n = 11 from 3 aged APP/PS1 mice, n = 15 from 3 aged NC mice, n = 16 from 3 adult APP/PS1 mice, n = 13 from 2 adult NC mice, and n = 12 from 3 adult C57BL/6J mice. Sample size of images analyzed for saline-injected mice: CA1 = 13, CA3 = 13, and DG = 12 from 3 adult C57BL/6J mice. One-way ANOVA with Tukey Post Hoc test results are shown (*$p<0.05$; **$p<0.01$; ***$p<0.001$).
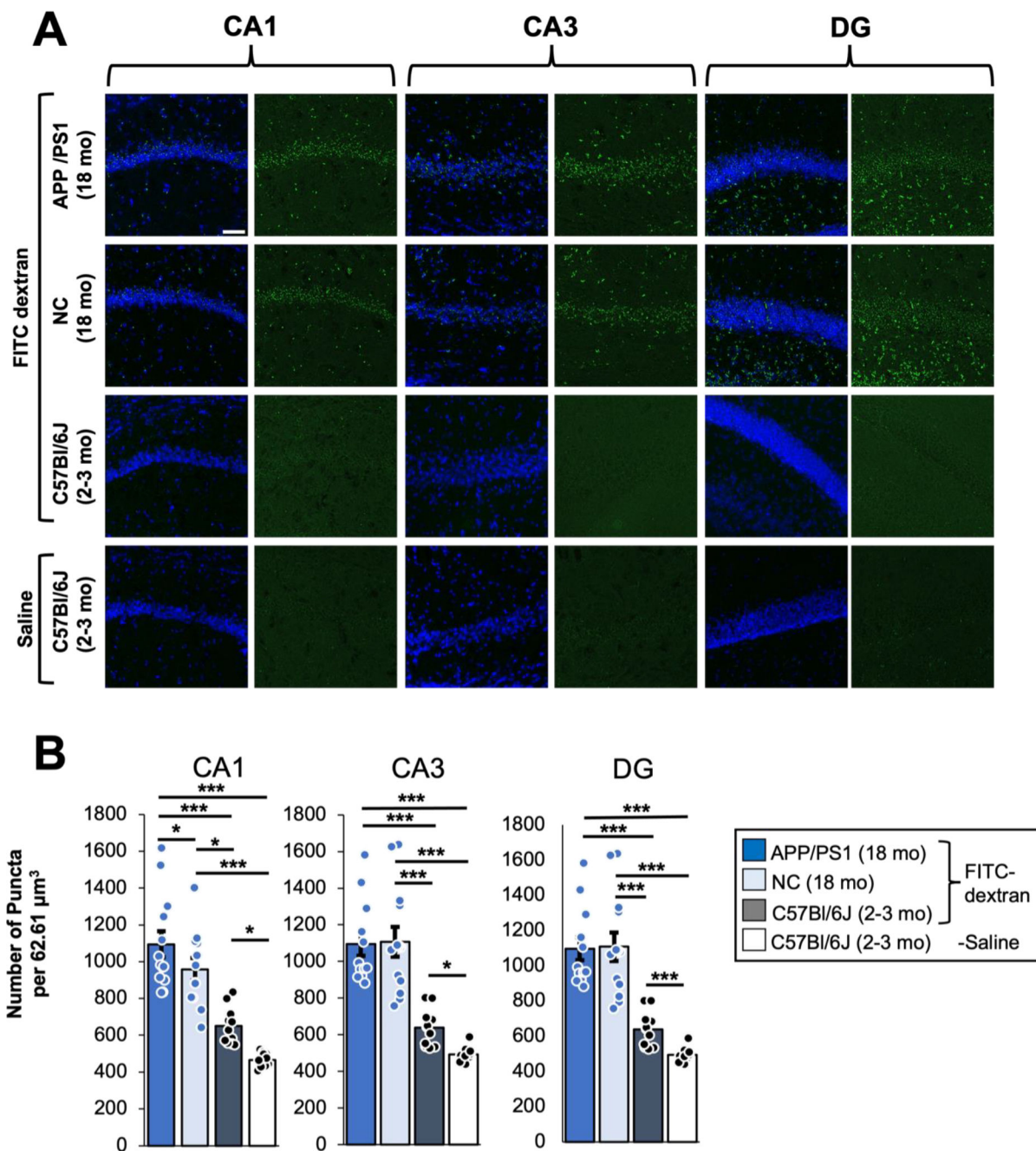
Figure 5. The BBB leakage are present in aged APP/PS1 mice and their control littermates but not young adult C57BL/6J mice.

Young adult C57BL/6J mice (1.5–2 mo old), aged APP/PS1 mice and their non-carrier (NC) control littermates (18 mo old) received an i.v. injection of 100 μl of FITC-dextran (50 mg/ml, MW 20 kDa,). A separate cohort of young adult C57BL/6J mice (2–3 mo old) received saline injection for negative control groups. After 1 h, mice were subjected to transcardial perfusion of PBS followed by fixation with 2% PFA. Cryoprotected brain tissues were sectioned to 30 μm coronal sections and counterstained with nuclear marker Hoechst 33342. Confocal z-stack images (an optical section of 1.0 μm) were collected from

the CA1, CA3, and Dente gyrus (DG) regions of the hippocampus. **(A)** Representative images showing a maximum projection z-stack of indicated brain regions for FITC-dextran. Scale bar: 50 μm. **(B)** Quantification of the background subtracted FITC fluorescence intensities within 90 μm^2 images which were maximum projected from the z-stack series using Fiji (ImageJ). 3-way ANOVA with age, genotype, and injection type as the three factors with post-hoc Fisher test results. Sample size: 12 z-project (1 μm z step) images between 2 individual mice per condition.